*J. Chem. Sci.* Vol. 124, No. 5, September 2012, pp. 969–978. 

# Electrochemical sensing and photocatalysis using Ag–$TiO_2$ microwires

SOUMIT S MANDAL and ANINDA J BHATTACHARYYA*
Solid State and Structural Chemistry Unit, Indian Institute of Science, Bangalore 560 012, India
e-mail: aninda_jb@sscu.iisc.ernet.in

MS received 11 August 2011; revised 1 March 2012; accepted 8 March 2012

**Abstract.** Anatase Ag–$TiO_2$ microwires with high sensitivity and photocatalytic activity were synthesized via polyol synthesis route followed by a simple surface modification and chemical reduction approach for attachment of silver. The superior performance of the Ag–$TiO_2$ composite microwires is attributed to improved surface reactivity, mass transport and catalytic property as a result of wiring the $TiO_2$ surface with Ag nanoparticles. Compared to the $TiO_2$ microwires, Ag–$TiO_2$ microwires exhibited three times higher sensitivity in the detection of cationic dye such as methylene blue. Photocatalytic degradation efficiency was also found to be significantly enhanced at constant illumination protocols and observation times. The improved performance is attributed to the formation of a Schottky barrier between $TiO_2$ and Ag nanoparticles leading to a fast transport of photogenerated electrons to the Ag nanoparticles.

**Keywords.** Ag–$TiO_2$ microwires; textile dyes; electrochemical sensing; photocatalysis; Schottky barrier.

## 1. Introduction

Nano-architectures of titania ($TiO_2$) possess several interesting optical and electronic properties[1] which make them promising for varied applications such as in catalysis,[2] sensors[3] and photovoltaic devices.[4,5] Nanostructuring provide increased area of interaction between the host $TiO_2$ and guest entity thus enhancing sensing or catalytic ability of $TiO_2$. It has been reported that substrate capabilities can be further enhanced by integrating it with metal or metal compound (e.g., oxides) particles. Specific examples are incorporation of carbon nanotubes (CNT) or graphene substrates with Cu,[6] Au,[7] Pt,[8] or CuO,[9] $RuO_2$.[10] Enhancement in performance has been attributed to surface and quantum size effects and also to interactions of substrate with metal/metal-oxide.[11] As sensing or photocatalytic properties are primarily based on redox processes involving charge (electron) transfer, coating with metal or metal-oxide trap electron states thus preventing electron-hole recombination. Coating with a metal such as Ag is expected to generate a composite material with high overall effective conductivity leading to significantly improved electron transfer kinetics between electrode and analyte. Electroanalytical methods of detection of analytes ranging from small molecular moieties to biomolecules using $TiO_2$ and metal-$TiO_2$ nanomaterials as substrates have received considerable attention. $TiO_2$ and noble metal-$TiO_2$ composites e.g., Pt–$TiO_2$ has been used in biosensors,[12] while bimetallic-nanoparticle $TiO_2$ materials have been used in various electrochemical and photoelectrochemical applications.[13] Noble metals such as Ag, Au, Pd and Pt have already found extensive usage in the field of sensors,[14] fuel cell,[15] catalysis[16] and as an antibacterial agents.[17] In the field of photodegradation of organic compounds such as organic dyes, the $TiO_2$-noble metal e.g., Ag–$TiO_2$ system is of immense importance and has been a subject of interest for last several years. Various studies have been carried out to investigate the role of Ag in the photocatalysis as well as optimize the concentration of Ag for achieving enhanced performance.[18–26] However, there are several persisting problems concerning catalyst cyclability, separation of catalyst from the degrading medium which downgrades catalyst performance. In addition to this, the detection limit of the systems for these compounds has never been taken up as a subject of interest. In this manuscript, we attempt to minimize the detrimental effects attached with above issues using Ag–$TiO_2$ microwires. In literature, several techniques (e.g., flame-spray synthesis,[27] electrodeposition,[28] sonochemical,[29] laser pyrolysis[30]) have been described for the synthesis of Ag–$TiO_2$. However, most of these techniques involve stringent synthesis conditions and procedures. Uniform distribution of nanoparticles on $TiO_2$ surface is a non-trivial issue and is

*For correspondence

difficult to control. Further, in certain cases the presence of Ag nanoparticles induce phase transformation in $TiO_2$.[23] This work describes a simple room temperature chemical route carried out for the preparation of Ag–$TiO_2$. The synthesis involved attachment of the noble metal nanoparticles on the surface aminosilane (3-aminopropyltrimethoxysilane, abbreviated as APTMS) modified $TiO_2$ microwires grown using optimized polyol method. The Ag–$TiO_2$ microwires were utilized for electrochemical analysis and photocatalytic degradation of a cationic dye e.g., methylene blue, a cationic dye. The performance of the Ag–$TiO_2$ were compared *vis-a-vis* $TiO_2$ microwires. The synthesized Ag–$TiO_2$ microwires showed excellent photocatalytic properties and cyclability compared to commercial $TiO_2$ materials.

## 2. Experimental: materials and methods

### 2.1 *Starting materials and synthesis of titania microwires*

Titanium (IV) tetraisopropoxide (TTIP), 3-aminopropyltrimethoxysilane (APTMS) were obtained from Sigma Aldrich. Tri-sodium citrate, silver nitrate, sodium borohydride, ethylene glycol (EG) and methylene blue (MB) were obtained from S.D. Fine Chemicals Ltd., India. Ethylene glycol (EG) was distilled prior to the preparation and stored under inert nitrogen atmosphere until further usage. $TiO_2$ microwires were prepared by polyol method. Briefly, 0.050 ml (~0.147 mmol) TTIP was added to 50 ml of EG under nitrogen gas flow in a sealed glove bag (Sigma). The solution was then taken out of the glove bag and heated to 170°C for 2 h under constant stirring. Following cooling down to room temperature, the white flocculate was separated via centrifugation and then washed with deionized water and ethanol several times for complete removal of excess EG from the sample. Dry titanium glycolate microwires were obtained by heating the precipitate under vacuum at 50°C for 4 h. Calcination of the glycolate microwires at 500°C for 3 h in a muffle furnace resulted in the formation of titania ($TiO_2$) microwires.

### 2.2 *Synthesis of titania-silver composite microwires*

Ag nanoparticles were synthesized according to the method reported in ref. 31. $TiO_2$ microwires of 0.2 g were at first functionalized with APTMS (using a solution of 300 µl of APTMS in 100 ml methanol).[32] This reaction was carried out overnight and the functionalized microwires were then dried at 50°C and added into a colloidal solution of the silver nanoparticles (prepared by the reduction of $AgNO_3$ using synthesis procedure as in ref. 31) and stirred slowly for 6 h. The above solution was centrifuged, washed with water three times and then dried for further characterization and use.

### 2.3 *Characterization for probing $TiO_2$ and $TiO_2$–Ag microwires morphology, structure*

Morphology of the $TiO_2$ and $TiO_2$–Ag microwires and the extent of dye adsorption on the microwires were characterized using transmission/scanning electron microscope (TEM), powder X-ray diffraction (XRD), Fourier transform infrared (FTIR) spectroscopy, thermogravimmetry analysis (TGA) and $N_2$ adsorption/desorption isotherms. Transmission electron microscope (FEI Tecnai F30) images were recorded with an acceleration voltage of 200 kV with $TiO_2$/Ag–$TiO_2$ cast on a Cu grid with carbon-reinforced plastic film. Scanning electron microscopy (FEI SIRION) was done in the voltage range of 200–300 kV. *X*-ray diffraction patterns (X'pert Pro Diffractometer, Phillips, Cu $K_\alpha$ radiation) were recorded in the $2\theta$ range from 5° to 65° at a scanning rate of 1° $min^{-1}$. X-ray photoelectron spectra (XPS) of Ag–$TiO_2$ were recorded on a Thermo Fisher Scientific Multilab 2000 (England) instrument with Al K$\alpha$ radiation (1486.6 eV). The binding energies reported here are with reference to graphite at 284.5 eV having an accuracy of ±0.1 eV. XPS data was recorded on pellets with 30% (w/w) graphite powder (no noticeable charging of the oxide samples was observed). Raman spectroscopy was carried out using a Fourier transform-Raman (FT-Raman) spectrometer (Thermonicolet, Thermoelectron Corporation) having a Hg–Cd–Te detector cooled to a liquid nitrogen temperature. An incident laser wavelength of 1064 nm was used as the source. Thermogravimmetry analysis (TGA, Perkin Elmer Pyris6000) experiments were done by heating the sample in a silica crucible from 30 to 700°C at a heating rate of 10°C $min^{-1}$ in $N_2$ atmosphere. For $N_2$ adsorption/desorption (Belsorp-Max) experiments the microwires were degassed at 150°C for 5 h. The dye adsorption kinetics were studied using uv-vis absorption spectroscopy (Perkin-Elmer, Lambda 35 UV Spectrometer, path length = 1 cm). 0.1 g of Ag–$TiO_2$ (microwires) was added to 100 ml (of 50 ppm, say) MB dye solution and stirred continuously for 2 h for homogeneity. Aliquots were collected from the reaction beaker at different time intervals and concentration of dye in solution as a function of time was determined by

monitoring the changes in the $\lambda_{max}$ line intensity with time.

### 2.4 *Electrochemical measurements for sensing dye content in aqueous solution: Preparation of modified electrode*

The glassy carbon electrode was coated with the $TiO_2$/Ag–$TiO_2$ composite microwires using a standard droplet evaporation procedure described in refs. 33–36. Firstly, Ag–$TiO_2$ water solution (10 mg of titania per ml of water) was prepared and adequately vortexed. Glassy carbon electrode (GCE, diameter: 3 mm) was polished with 0.3 μm alumina slurry to a mirror finish. After each polishing step, the electrode was rinsed and ultrasonicated, respectively in ethanol and redistilled water for 60 s. 20 μl of aqueous titania solution was dropped on the shining surface of GCE and dried for 3–4 h in air at room temperature (25°C). This GCE–$TiO_2$/Ag–$TiO_2$ comprised of the working electrode of the three electrode cell.

### 2.5 *Cyclic voltammetry for dye detection*

The electrochemical response of the dye in solution was estimated using cyclic voltammetry (CH608C, CH Instruments). The working, counter and reference electrodes were $TiO_2$/GCE, platinum wire and saturated calomel electrode (SCE), respectively. The electrodes were dipped in 5 ml of dye-deionised water solution having varying dye concentrations (approximately: 15–100 ppm). The solution was deoxygenated for 30 min prior to the start of the measurements and nitrogen atmosphere was maintained throughout the duration of the experiment.

### 2.6 *Photocatalytic degradation of dyes in aqueous solution*

The photochemical reactor used in this study was made of a Pyrex glass jacketed quartz tube. A high pressure mercury vapour lamp (HPML) of 125 W (Philips, India) was placed inside the jacketed quartz tube. To avoid fluctuations in the input light intensity, supply ballast and capacitor were connected in series with the lamp. Water was circulated through the annulus of the quartz tube to avoid heating of the solution. The solution of 100 ml was taken in the outer reactor and continuously stirred to ensure that the suspension of the catalyst was uniform. The lamp radiated predominantly at 365 nm corresponding to energy of 3.4 eV and photon flux of $5.8 \times 10^{-6}$ mol of photons/s. For the photocatalysis experiments with Ag–$TiO_2$ microwires, three concentrations of MB dye (20 ppm, 30 ppm and 50 ppm, all in 100 ml) were used (0.1 g of $TiO_2$ in 100 ml of dye solution).

## 3. Results and discussion

Figure 1a–c show the transmission electron microscope (TEM) images of titania microwires obtained from intermediate titanium glycolate microwires via the synthesis procedure described in section 2. The approximate length and diameter of the microwires are 3 μm and 0.8 μm, respectively. For Ag–$TiO_2$ composite microwires (figure 1a and b) TEM revealed numerous isolated dark spots as well as connected clusters of dark spots spread over the surface of $TiO_2$ microwires suggesting successful attachment of Ag particles on the $TiO_2$ microwires. It is envisaged that the Ag trapping on the $TiO_2$ surface takes place via electrostatic attractive forces.[37] The amine

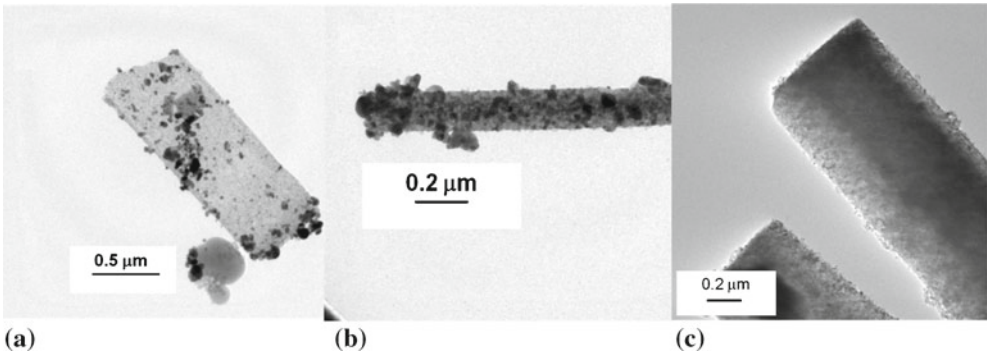


**Figure 1.** Transmission electron micrographs showing the solid wire like morphology of (**a**) and (**b**) Ag–$TiO_2$ composite nanowires. Black spots (clusters of spots) on the surface of microwires represent the grafted Ag. (**c**) Bare as synthesized $TiO_2$ microwires.

functionalised $TiO_2$ microwires carry positive charges which trap the negatively charged citrate stabilised Ag nanoparticles.

The X-ray diffraction pattern of the synthesized $TiO_2$ microwires (figure 2a) could be completely indexed to anatase phase (JCPDS file no. 21–1272).[38] The crystallite size (d) estimated from the full width at half maximum ($w$) of the dominant (101) peak at diffraction angle $2\theta \approx 25.2°$ using Scherrer's equation was approximately 19 nm. Functionalization with $NH_2$ did not result in additional peaks suggesting identical anatase structure as pristine $TiO_2$. As a consequence of silver deposition on the $TiO_2$ surface, enhancement in peak intensities are observed. Due to the presence of Ag on the $TiO_2$ surface additional peaks appear at $2\theta \approx 38.2°$, 44.3° and 64.5°. The main diffraction peak of Ag at 38.2° could not be independently observed due to significant overlap with the anatase $TiO_2$ peak at 37.1°. Before sintering, Ti-glycolate microwires are amorphous. The peaks corresponding to $TiO_2$ emerge only following sintering signifying the formation of crystalline $TiO_2$. Raman spectra (figure 2b) further support the results of XRD. The Raman peaks at 148, 401, 521 and 642 $cm^{-1}$ can be attributed to the five Raman active modes of the anatase phase[39] with the symmetries of $E_g$, $B_{1g}$, $A_{1g}$ and $E_g$, respectively (figure 2b). Functionalization of $TiO_2$ did not result in any new bands suggesting overall retention of the $TiO_2$ anatase structure.

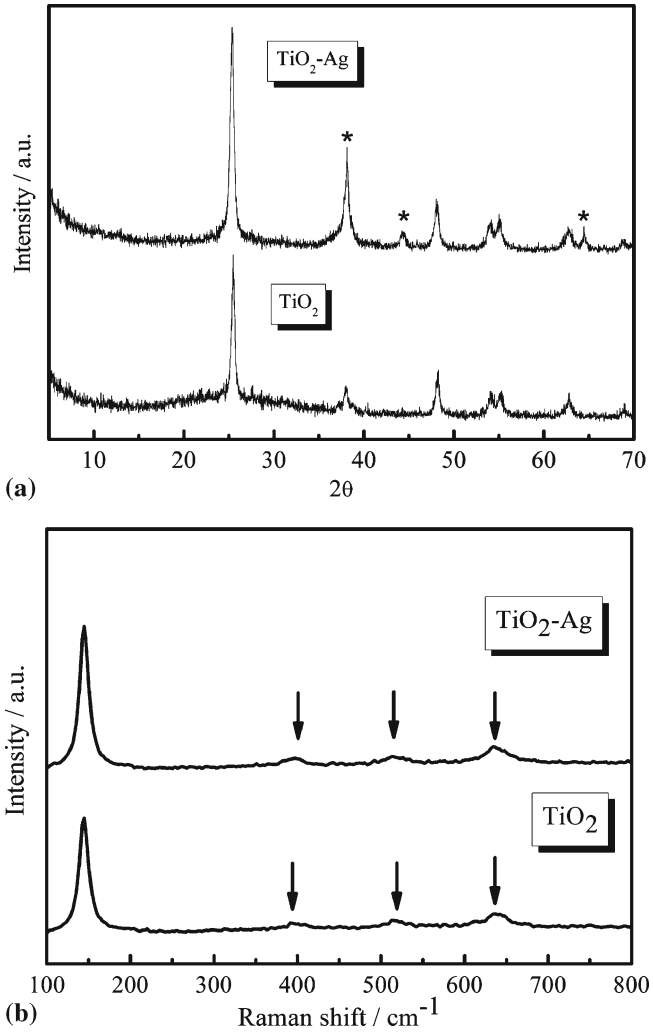


**Figure 2.** X-ray diffraction pattern of (**a**) anatase $TiO_2$ and Ag–$TiO_2$ composite microwires. The Ag peaks have been marked using (*). (**b**) Raman spectra of bare $TiO_2$ microwires and Ag–$TiO_2$.

XPS was employed for the surface analysis of the Ag–$TiO_2$ sample. Figure 3a depicts the full XPS spectrum of Ag–$TiO_2$. It contains three major peaks from O-1s (figure 3d), Ti-2p and Ag-3d states. The XPS spectrum for Ag (figure 3b) gives binding energy of Ag (3d) at 368 eV and 374 eV corresponding to Ag($3d_{5/2}$) and Ag($3d_{3/2}$). These values indicate that Ag is present on the $TiO_2$ surface as Ag(0) i.e., in the metallic state.[40] The XPS spectra of Ti (figure 3c) shows two peaks located at 463.72 eV corresponds to Ti-$2p_{1/2}$ and another one located at 458.05 eV is assigned to Ti $2p_{3/2}$. The splitting between Ti-$2p_{1/2}$ and Ti-$2p_{3/2}$ is 5.6 eV, indicating a normal state of $Ti^{4+}$ in the as-prepared mesoporous anatase $TiO_2$.[40]

$N_2$ adsorption/desorption were performed to measure the surface area of the as-synthesized Ag–$TiO_2$ microwires (figure 4). Significant degree of hysteresis was also observed between the adsorption and desorption isotherms. The nature of the isotherms strongly suggests the presence of mesoporosity on the Ag–$TiO_2$ microwires surface. The surface area of Ag–$TiO_2$ was 17.9 $m^2\,g^{-1}$ which is less than half of pristine $TiO_2$ ($\approx$43 $m^2\,g^{-1}$). The decrease in surface area is attributed to blocking of the pores by the Ag particles. This explains the difference in the isotherm between the $TiO_2$ and Ag–$TiO_2$.

Figure 5 shows $\lambda_{max}$ (from UV-vis spectroscopy; 200–700 nm) line intensity variation as a function of time for various MB concentrations in solution. The concentration of the Ag nanoparticles on the $TiO_2$ surface was estimated to be approximately $3.033 \times 10^{-2}$ mM from the calibration curve obtained from recording the $\lambda_{max}$ of varying concentration of the silver colloidal solution. It was observed that the colour intensity of the MB–Ag–$TiO_2$ solution decreased progressively over a period of approximately 60 min when the Ag–$TiO_2$ wires were dispersed into the MB solution. Beyond 60 min, the concentration of the dye in the solution remained almost same. The decrease in concentration due to adsorption of dye is lesser for Ag–$TiO_2$ compared to pristine $TiO_2$. This is attributed to

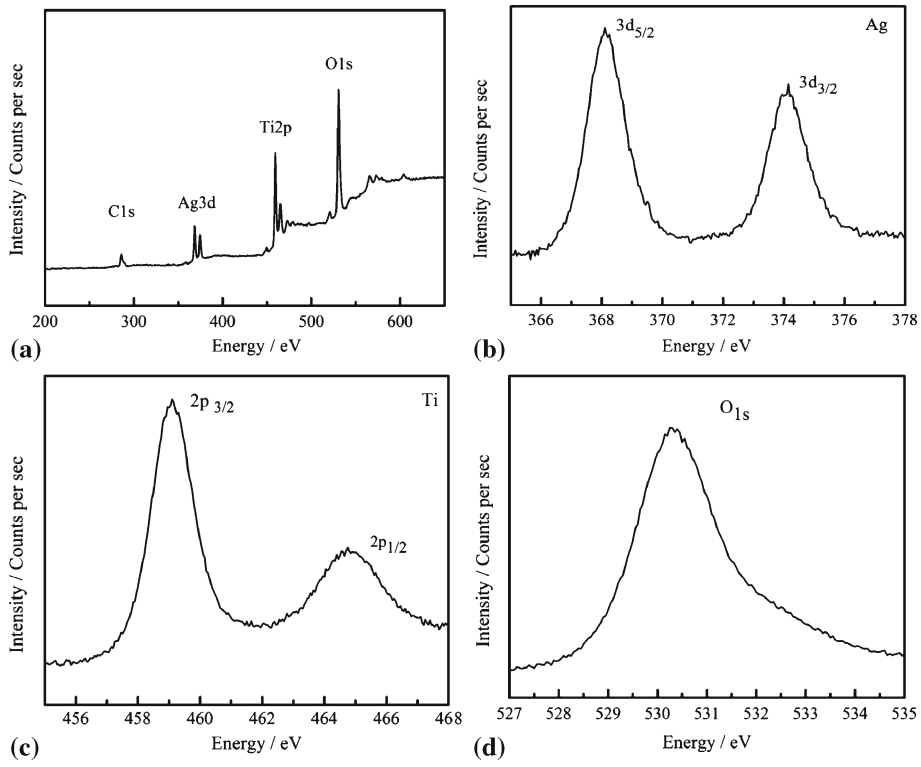


**Figure 3.** XPS pattern of Ag–$TiO_2$ nanowires. (**a**) Full spectrum, (**b**) Ag-3d, (**c**) Ti-2p, (**d**) O-1s.

the decrease in surface area of the Ag–$TiO_2$ microwires compared to $TiO_2$.

### 3.1 *Electrochemical detection of methylene blue (MB) in solution using $TiO_2$/Ag–$TiO_2$ microwires*

The drop casted $TiO_2$/Ag–$TiO_2$ film has an estimated thickness of approximately 5 μm. Photographic visualization (not shown here) showed that the $TiO_2$/Ag–$TiO_2$ coverage remained same before and after the cyclic voltammetry experiments. Figure 6 shows the electrochemical response of Ag–$TiO_2$/GCE and $TiO_2$/GCE systems in aqueous solution of MB

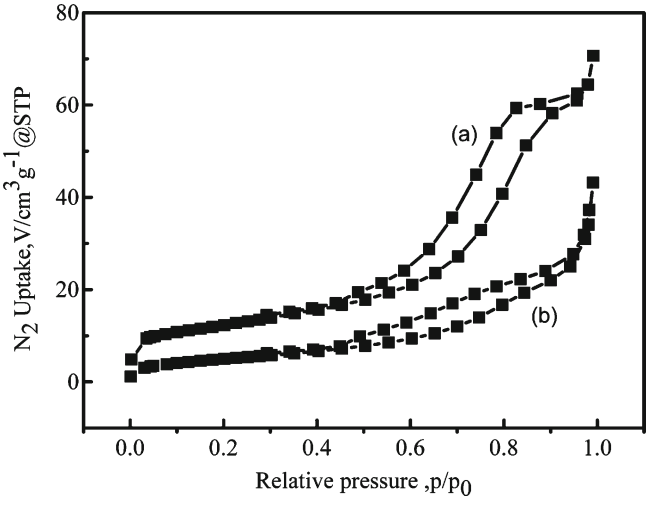


**Figure 4.** $N_2$ adsorption/desorption isotherms of (a) $TiO_2$, (b) Ag–$TiO_2$ composite nanowires.

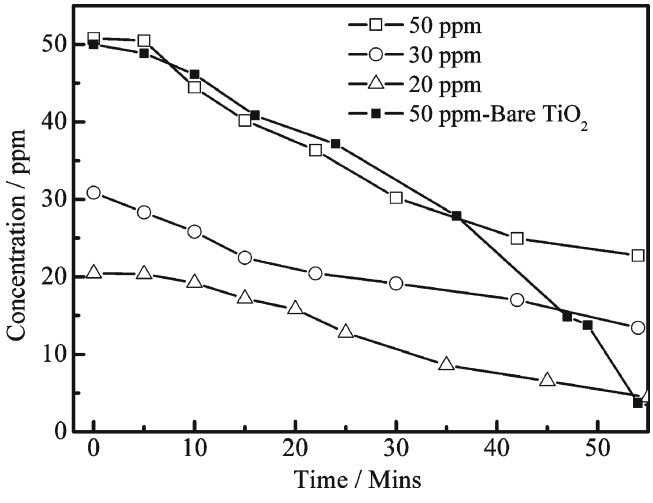


**Figure 5.** Variation in solution dye concentration (absorption) versus time as a result Ag–$TiO_2$ microwires dispersion in a solution having different initial MB concentrations: (□) 50 ppm, (◯) 30 ppm, (△) 20 ppm. Filled squares (■) show the adsorption by the bare $TiO_2$ nanowires while unfilled symbols show the adsorption due to Ag–$TiO_2$ microwires.

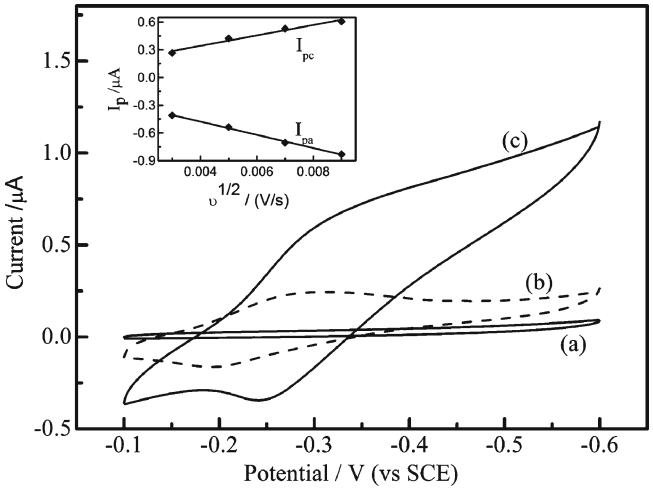


**Figure 6.** Cyclic voltammogram of (a) bare GCE, (b) $TiO_2$/GCE, (c) Ag–$TiO_2$/GCE at a scan rate of 0.01 $Vs^{-1}$ (T = 25°C, 50 ppm). Inset: variation of $I_{pc}$ and $I_{pa}$ versus scan rates.

dye. It was found that for the same dye concentration (≈ 50 ppm) redox peak currents were higher approximately 2–2.5 times in magnitude for Ag–$TiO_2$ compared to bare $TiO_2$ microwires[41] (anodic peak: 2.1; cathodic peak: 2.54). Both cathodic and anodic peaks for Ag–$TiO_2$ exhibit a slight shift with respect to bare $TiO_2$. The cathodic and anodic peaks for Ag–$TiO_2$ appear at −0.302 V (shift of 0.0073 V) and −0.242 V (shift of 0.049 V). The electrode reaction of MB involves two successive one-electron charge transfer coupled with a rapid reversible protonation between $MB^+$ and leucomethylene blue (LMB).[42] The improved current response in case of Ag–$TiO_2$ microwires can be ascribed to the presence of Ag which increases the overall effective conductivity of composite (i.e., Ag–$TiO_2$) resulting in better electron transfer between the analyte molecule and electrode and thus enhancing detection capability and sensitivity of the Ag–$TiO_2$ system.[12,13] Due to this enhanced electron transfer between the dye molecule and the electrode surface, the reduction reaction takes place at a much lower reduction potential value leading to the shift in the position of the anodic peak. Also, it was found that with an increasing scan rate, the redox peak currents of MB increased linearly as function of the square root of the scan rate. This observation suggests a diffusion controlled process.

Figure 7 shows the cyclic voltammograms of Ag–$TiO_2$ (length: 3 μm and diameter = 0.8 μm)/GCE electrode system in aqueous solutions with different initial concentrations of MB (15–100 ppm). The study was performed to estimate the sensitivity of the Ag–$TiO_2$ microwires for possible use as substrates in

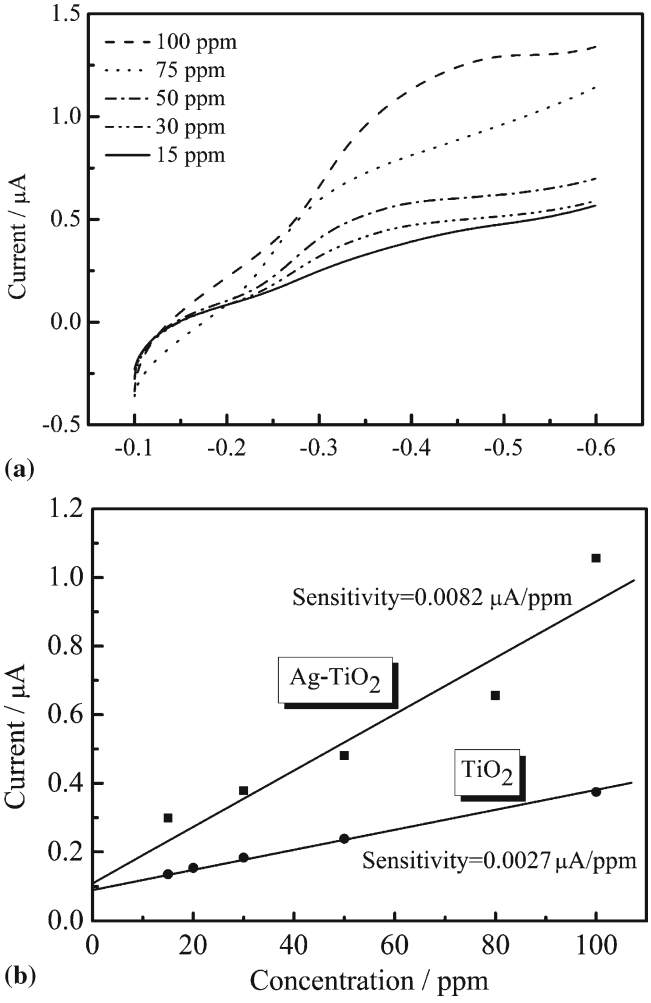


**Figure 7.** (**a**) Cyclic voltammogram of Ag–$TiO_2$ with MB concentrations varying from 15 to 100 ppm. (**b**) The variation of anodic current with MB concentration, scan rate 0.01 $Vs^{-1}$ for $TiO_2$ and Ag–$TiO_2$ system.

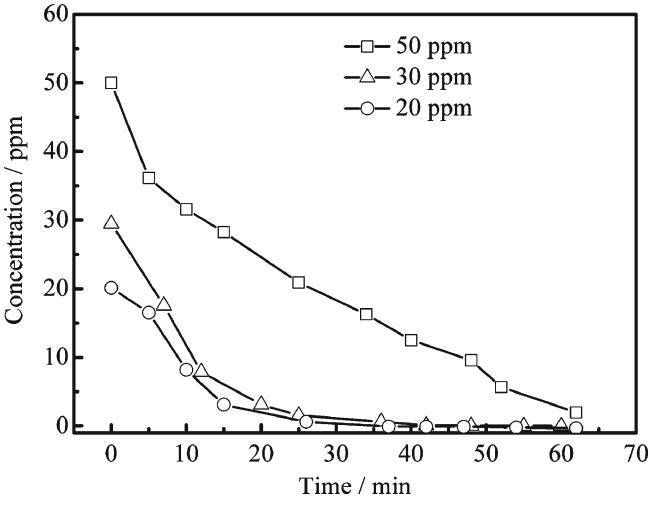


**Figure 8.** Photocatalysis of methylene blue carried out using 0.1 g of $TiO_2$ microwires and Ag–$TiO_2$ per 100 ml of dye solutions for 50, 30 and 20 ppm dye solution.

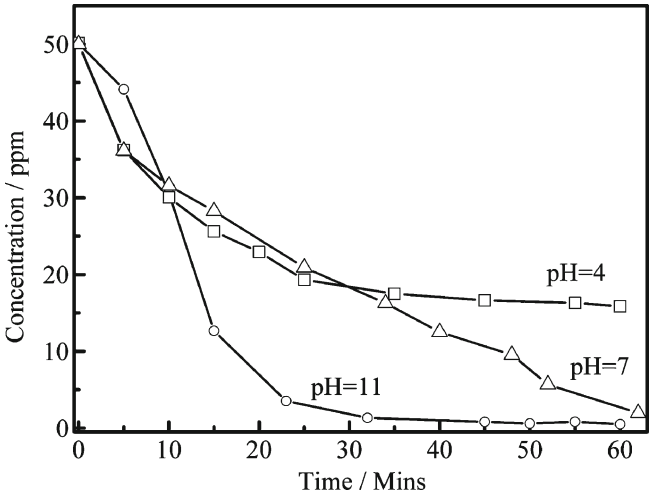


**Figure 9.** Photocatalysis of methylene blue carried out using 0.1 g of Ag–$TiO_2$ microwires per 100 ml of dye solutions at pH 5, 7 and 11.

practical sensors for detection of cationic industrial dyes. The cathodic current corresponding to the peak at −0.3023 V (figure 7a) increased linearly with increasing initial concentration of MB in solution. Employing a linear fit to current versus initial solution dye concentration data (figure 7b) the sensitivity was estimated to be approximately 0.00813 $\mu Appm^{-1}$. The Ag–$TiO_2$ sensitivity was observed to be more than thrice that of bare $TiO_2$ microwires system 0.003 $\mu Appm^{-1}$ (not shown here).[41] The increase in sensitivity is attributed to the improved conductivity of the Ag–$TiO_2$ compared to $TiO_2$ as discussed earlier.

### 3.2 *Photocatalytic degradation of methylene blue (MB) by Ag–$TiO_2$ microwires at various pH*

The $TiO_2$ and Ag–$TiO_2$ were observed to perform well as substrates for degradation of methylene blue (MB). The presence of Ag on $TiO_2$ resulted in additional enhancement in degradation of dyes. 0.1 g of Ag–$TiO_2$ microwires in 20 ppm/30 ppm/50 ppm in 100 ml solution was repeatedly illuminated for 5 min at 2 min intervals. During the 2 min interval, 1 ml aliquots were obtained from the test mixture. Due to progressive degradation of the dye with consecutive, flashes, the colour of the solution mixture (as well as aliquots) changed from blue to light blue to finally white. The change in dye solution colour or dye degradation as a function of time was monitored using uv-vis spectroscopy. For all initial solution MB concentrations (20–50 ppm), $\lambda_{max}$ line intensity decreased with varying rates to negligibly small values over a period of 60 min. However, the rate at which the dye degraded was much faster in case of Ag–$TiO_2$ (figure 8) compared to bare $TiO_2$ microwire.[41] This suggests that Ag–$TiO_2$ microwires are highly efficient substrates for the degradation of azo dyes such as methylene blue (MB) and the presence of silver on the $TiO_2$ substrates enhances the degradation of the dye. Figure 9 shows the photocatalytic degradation of the methylene blue as a function of pH of solution. The dye adsorption and degradation depend heavily on the state of the surface and pH is one of the important parameters affecting the surface state.[43] Drastic changes were observed in the kinetics performed at various pH (figure 9) viz.

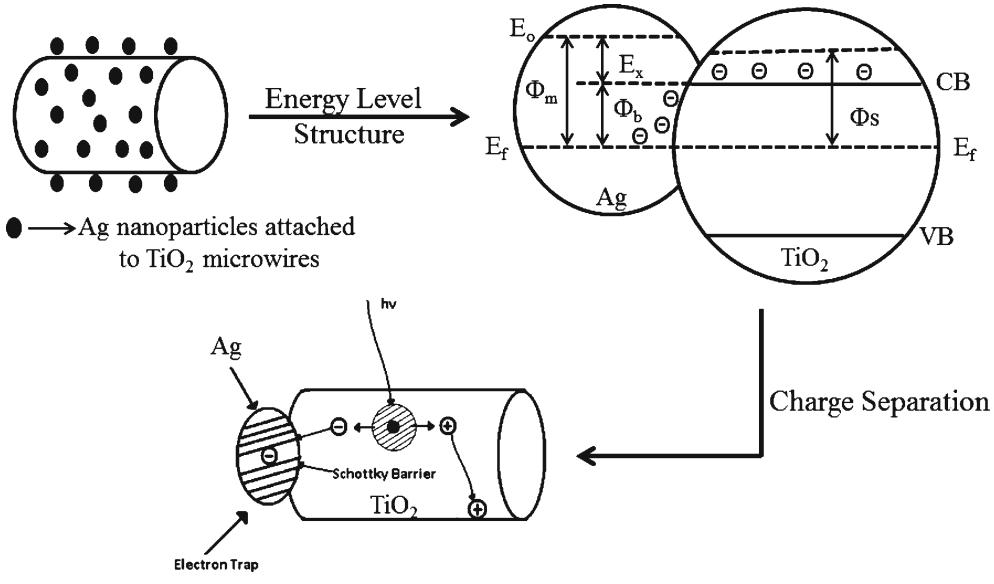


**Figure 10.** Schematic depiction of Schottky barrier and charge separation in metal attached semiconductors.

pH = 4, 7, 11. While in alkaline solutions (pH = 11) MB degraded at a faster rate with the dye concentration decreasing to a very low value in ≈ 30 min, in acidic solutions (pH = 4) the rate became slower and degree of degradation was lower in the same time period. Thus, we observe that Ag–$TiO_2$ microwires had excellent photocatalytic ability at varying pH ranges. The better photocatalytic ability of the Ag–$TiO_2$ microwires systems can be explained using the concept of the formation of the Schottky barrier[44] at the silver–titania junction. Metals (such as Ag) and the semiconductor ($TiO_2$) possess different Fermi level positions. The presence of the silver on the $TiO_2$ surface leads to the formation of the Schottky barrier as shown in the figure 10. The electron migration from the $TiO_2$ to the Ag occurs until the two Fermi levels are aligned since the Ag has a work function ($\Phi_m$) higher than that of the $TiO_2$ ($\Phi_s$). The surface of the Ag acquires an excess negative charge, while the $TiO_2$ exhibits an excess positive charge as a result of electron migration away from the barrier region. A Schottky barrier forms at the Ag–$TiO_2$ interface. The height of the barrier ($\Phi_b$) is defined as the difference between the $TiO_2$ conduction band and the Ag Fermi level. This Schottky barrier formed at the Ag–$TiO_2$ interface can serve as an efficient electron trap to avoid the electron-hole recombination in the photocatalytic process. Figure 10 illustrates the mediating role of Ag in storing and shuttling photo-generated electrons from the $TiO_2$ to an acceptor in a photocatalytic process. Thus, the photo-induced electrons in the conduction band of the semiconductor are believed to readily transfer to the metal, which facilitates the separation of the photo-induced electron-hole pairs and effectively inhibits their recombination. The Ag particles distributed on the surface of the $TiO_2$ could greatly enhance the overall photocatalytic efficiency.

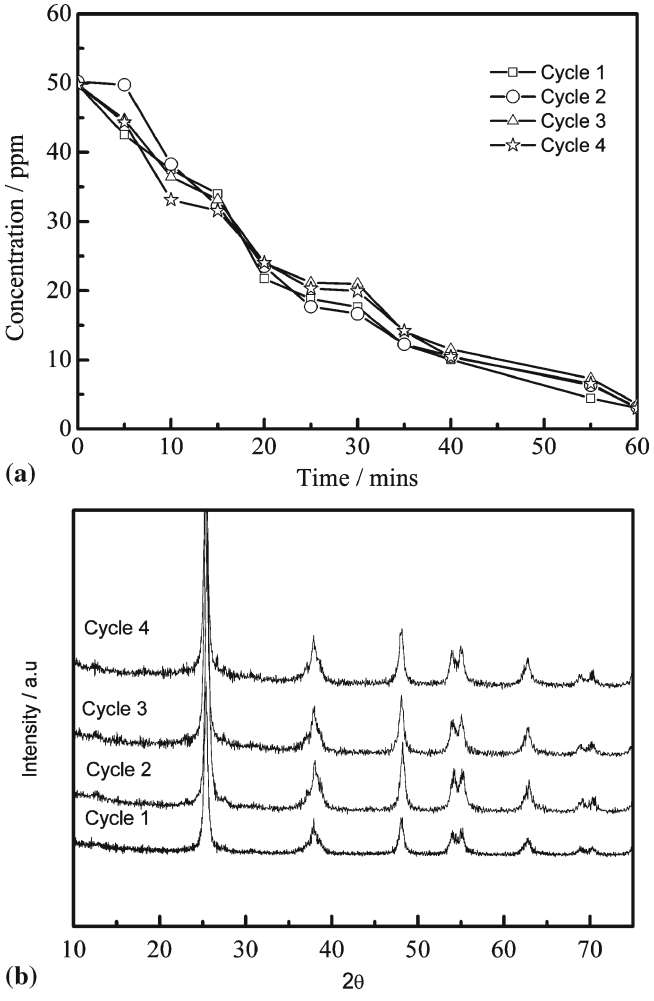


**Figure 11.** (**a**) Photocatalysis of MB carried out four times under UV irradiation using the same Ag–$TiO_2$ microwires, (**b**) XRD pattern of the Ag–$TiO_2$ following repeated (four times) photocatalytic cycling.

To investigate the stability of the Ag–$TiO_2$ composite microwires on the photocatalytic activity under UV irradiation, the samples were repeatedly used four times after separation via filtration and repeated washing with water and ethanol until a clear supernatant was obtained. The degradation of the dye in each cycle was found to be same as seen in figure 11a. Thus, the Ag–$TiO_2$ photocatalyst was found to be stable for repeated use under UV irradiation. The XRD pattern of the Ag–$TiO_2$ sample was also recorded after each cycle. As seen in figure 11b, the peaks corresponding to anatase $TiO_2$ as well as Ag are detected in the XRD patterns but with reduced intensities. The XPS spectra of the Ag–$TiO_2$ samples (supplementary information) recorded after photocatalytic cycling shows the presence of Ag. Thus, the XRD and XPS results are consistent with the repeated photocatalytic degradation and the Ag nanoparticles play an important role in improving the photocataytic activity of the $TiO_2$–Ag composites.

## 4. Conclusions

In summary, we have presented here a simple polyol method followed by a surface modification approach for the synthesis of high aspect ratio (≈ 4) $TiO_2$–Ag composite mesoporous microwires. The surface modified $TiO_2$ microwires facilitate loading of Ag nanoparticles on $TiO_2$ surface. The $TiO_2$–Ag not only possess enhanced detection limit and photocatalytic activity, but also possess higher cyclability in comparison to $TiO_2$/$TiO_2$–Ag systems of prior art. Ag–$TiO_2$ also

showed better photocatalytic activity in a wide pH range. These features combined with the biocompatibility of $TiO_2$–Ag system make them attractive as substrates in biosensors for sensing of biological analytes. The Ag–$TiO_2$ systems described here will also be useful for waste water purification as well as detection of toxic entities in aqueous conditions. Apart from environmental applications, the present Ag–$TiO_2$ microwires following suitable morphological optimization will be promising for electrochemical applications such as electrodes in rechargeable lithium batteries.[45]

## Supplementary information

The supplementary information can be seen in www.ias.ac.in/chemsci.

## Acknowledgements

The authors thank I S Jarali (SSCU, Indian Institute of Science (IISc.), Bangalore) for TGA and BET measurements, Surat Kumar (INI, IISc., Bangalore) for TEM, and Sanjit Mahesh (IPC, IISc, Bangalore) for Raman spectra, and Sanjit Parida (SSCU, IISc, Bangalore) for XPS measurement. AJB acknowledges the Department of Science and Technology (DST), New Delhi and DST Nano Mission, Govt. of India for financial support.

## References

1. Chen X, and Mao S S 2007 *Chem. Rev.* **107** 2891
2. Borgarello E, Kiwi J, Pelizzetti E, Visca M and Gratzel M 1981 *Nature* **289** 158
3. Shu X, Chen Y, Yuan H, Gao S and Xiao D 2007 *Anal. Chem.* **79** 3695
4. Mor G K, Kim S, Paulose M, Varghese O K, Shankar K, Basham J and Grimes C A 2009 *Nano Lett.* **9** 4250
5. Chen J S, Tan Y L, Li C M, Cheah Y L, Luan D, Madhavi S, Boey F Y C, Archer L A and Lou X W 2010 *J. Am. Chem. Soc.* **132** 6124
6. Kang X, Mai Z, Zou X, Cai P and Mo J 2007 *Anal. Biochem.* **363** 143
7. Guo Y, Guo S, Fang Y and Dong S 2010 *Electrochim. Acta* **55** 3927
8. Rong L-Q, Yang C, Qian Q-Y and Xia X-H 2007 *Talanta* **72** 819
9. Zhuang Z, Su X, Yuan H, Sun Q, Xiao D and Choi M M F 2008 *Analyst* **133** 126
10. Ye J S, Cui H, Liu X, Lim T, Zhang W D and Sheu F S 2005 *Small* **1** 560
11. Li H, Bian Z, Zhu J, Huo Y, Li H and Lu Y 2007 *J. Am. Chem. Soc.* **129** 4538
12. Wen D, Guo S, Zhai J, Deng L, Ren W and Dong S 2009 *J. Phys. Chem.* **C 113** 13023
13. Wen D, Guo S, Wang Y and Dong S 2010 *Langmuir* **26** 11401
14. Ahmadalinezhad A, Kafi A K M and Chen A 2009 *Electrochem. Commun.* **11** 2048
15. Wang S, Jiang S P, White T J, Guo J and Wang X 2009 *J. Phys. Chem.* **C 113** 18935
16. Xu J, White T, Li P, He C, Yu J, Yuan W and Han Y-F 2010 *J. Am. Chem. Soc.* **132** 10398
17. Fabrega J, Fawcett S R, Renshaw J C and Lead J R 2009 *Environ. Sci. Tech.* **43** 7285
18. Herrmanna J-M, Tahiri H, Ait-Ichou Y, Lassaletta G, González-Elipe A R and Fernández A 1997 *Appl. Catal.* **B 13** 219
19. Arabatzis I M, Stergiopoulos T, Bernard M C, Labou D, Neophytides S G and Falaras P 2003 *Appl. Catal.* **B 42** 187
20. Vamatheva V, Amal R, Beydoun D, Low G and McEvoy S 2002 *J. Photochem. Photobiol. A: Chem.* **148** 233
21. Sclafani A and Herrmann J-M 1998 *J. Photochem. Photobiol. A: Chem.* **113** 181
22. Stathatos E, Lianos P, Falaras P and Siokou A 2000 *Langmuir* **16** 2398
23. Yu J, Xiong J, Cheng B and Liu S 2005 *Appl. Catal.* **B 60** 211
24. Sung-Suh H M, Choi J R, Hah H J, Koo S M and Bae Y C 2004 *J. Photochem. Photobiol. A: Chem.* **163** 37
25. Guo G, Yu B, Yu P and Chen X 2009 *Talanta* **79** 570
26. Ren L, Zeng Y-P and Jiang D 2009 *Catal. Commun.* **10** 645
27. Teoh W-Y, Mädler L, Beydoun D, Pratsinis S E and Amal R 2005 *Chem. Eng. Sci.* **60** 5852
28. Francioso L, Presicce D S, Siciliano P and Ficarella A 2007 *Sens. Actuators B: Chem.* **123** 516
29. Mizukoshi Y, Makise Y, Shuto T, Hu J, Tominaga A, Shironita S and Tanabe S 2007 *Ultrason. Sonochem.* **14** 387
30. Giraud S, Loupias G, Maskrot H, Herlin-Boime N, Valange S, Guélou E, Barrault J and Gabelica Z 2007 *J. Eur. Ceram. Soc.* **27** 931
31. Jana N R, Gearheart L and Murphy C J 2001 *Chem. Commun.* **617**
32. Kapoor S, Hegde R and Bhattacharyya A J 2009 *J. Control. Release* **140** 34
33. Durst R A, Bäumner A J, Murray R W, Buck R P and Andrieux C P 1997 *Pure Appl. Chem.* **69** 1317
34. Garguilo M G, Huynh N, Proctor A and Michael A C 1993 *Anal. Chem.* **65** 523
35. Liu Y, Wu S, Ju H and Xu L 2007 *Electroanalysis* **19** 986
36. Li X, Zheng W, Zhang L, Yu P, Lin Y, Su L and Mao L 2009 *Anal. Chem.* **81** 8557
37. (a) Guo S J, Dong S J and Wang E K 2009 *Chem. Eur. J.* **15** 2416; (b) Cui R J, Liu C, Shen J M, Gao D, Zhu J J and Chen H Y 2008 *Adv. Funct. Mater.* **18** 2197
38. Zhong L-S, Hu J-S, Wan L-J and Song W-G 2008 *Chem. Commun.* 1184
39. Ohsaka T, Izumi F and Fujiki Y 1978 *J. Raman Spectrosc.* **7** 321
40. (a) In: D Briggs, M P Seah (eds), *Practical surface analysis*, New York: John Wiley and Sons (1983); (b) In: J F Moulder, W F Stickle, P E Sobol, K D Bomben (eds), *Handbook of X-ray photoelectron*

*spectroscopy*, Eden Prairie, MN: Perkin-Elmer Corporation Physical Electronics Division (1992)
41. Mandal S S and Bhattacharyya A J 2010 *Talanta* **82** 876
42. (a) Kara P, Kerman K, Ozkan D, Meric B, Erdem A, Ozkan Z and Ozsoz M 2002 *Electrochem. Commun.* **4** 705; (b) John S A, Ramaraj R 1996 *Langmuir* **12** 5689
43. (a) Fox M A and Dulay M T 1993 *Chem. Rev.* **93** 341; (b) Linsebigler A L, Lu G and Yates J T 1995 *Chem. Rev.* **95** 735; (c) Konstantinou I K and Albanis T A 2004 *Appl. Catal. B. Environ.* **49** 1
44. (a) Shan Z, Wu J, Xu F, Huang F-Q and Ding H 2008 *J. Phys. Chem.* **C 112** 15423; (b) Wang C, Yin L, Zhang L, Liu N, Lun N and Qi Y 2010 *ACS Appl. Mater. Interf.* **2** 3373; (c) Emilio C A, Litter M I, Kunst M, Bouchard M and Justin C C 2006 *Langmuir* **22** 3606; (d) Wu M-C, Sápi A, Avila A, Szabó M, Hiltunen J, Huuhtanen M, Tóth G, Kukovecz Á, Kónya Z, Keiski R, Su W-F, Jantunen H and Kordás K 2011 *Nano Res.* **4** 360
45. Das S K and Bhattacharyya A J 2011 *Mater. Chem. Phys.* **130** 569